

Amandolese, X., et al., Low speed flutter and limit cycle oscillations of a two-degree-of-freedom flat plate in a wind tunnel. Journal of Fluids and Structures (2013), <http://dx.doi.org/10.1016/j.jfluidstructs.2013.09.002i>

## **LOW SPEED FLUTTER AND LIMIT CYCLE OSCILLATIONS OF A TWO-DEGREE-OF-FREEDOM FLAT PLATE IN A WIND TUNNEL**

X. Amandolese<sup>1,2</sup>, S. Michelin<sup>1</sup> and M. Choquel<sup>1</sup>

<sup>1</sup> LadHyX, CNRS-Ecole Polytechnique, F-91128 PALAISEAU, France

<sup>2</sup> Département ISME, CNAM, Paris, France

Corresponding Author: Dr. X. Amandolese

LadHyX, CNRS-Ecole Polytechnique, F-91128 PALAISEAU, France

Email : [xavier.amandolese@ladhyx.polytechnique.fr](mailto:xavier.amandolese@ladhyx.polytechnique.fr)

Tel. : +33 1 69 33 52 86 Fax: +33 1 69 33 52 92

### **ABSTRACT**

This paper explores the dynamical response of a two-degree-of-freedom flat plate undergoing classical coupled-mode flutter in a wind tunnel. Tests are performed at low Reynolds number ( $Re \sim 2.5 \times 10^4$ ), using an aeroelastic set-up that enables high amplitude pitch-plunge motion. Starting from rest and increasing the flow velocity, an unstable behaviour is first observed at the merging of frequencies: after a transient growth period the system enters a low amplitude limit-cycle oscillation regime with slowly varying amplitude. For higher velocity the system transitions to higher-amplitude and stable limit cycle oscillations (LCO) with an amplitude increasing with the flow velocity. Decreasing the velocity from this upper LCO branch the system remains in stable self-sustained oscillations down to 85% of the critical velocity. Starting from rest, the system can also move toward a stable LCO regime if a significant perturbation is imposed. Those results show that both the flutter boundary and post-critical behaviour are affected by nonlinear mechanisms. They also suggest that nonlinear aerodynamic effects play a significant role.

### **KEYWORDS**

Low speed flutter, limit cycle oscillation, nonlinear aeroelasticity, wind tunnel, flat plate

## NOMENCLATURE

$a$	distance in semi-chord from the mid-chord to the elastic axis, $x_{CG}/b$
$b$	half chord of the flat plate model, $c/2$
$c$	chord of the flat plate model
$C_L$	aerodynamic lift coefficient, $L/(0.5\rho U^2 sc)$
$C_M$	aerodynamic moment coefficient, $M/(0.5\rho U^2 sc^2)$
$D_a$ $D_h$	viscous structural damping in pitch and plunge
$h$	position in plunge measured at the elastic axis (positive downward)
$h_0$	initial condition in plunge
$h_{LCO}$	amplitude in plunge at LCO
$I_a$	inertia of the moving parts about the elastic axis
$K_a$ $K_h$	stiffness in pitch and plunge
$L$	aerodynamic lift force (positive upward)
$m$	mass of the moving parts
$M$	aerodynamic moment about the elastic axis (positive nose-up)
Re	Reynolds number, $Uc/\nu$
$r_g$	radius of gyration in semi-chords of the system about its elastic centre, $\sqrt{I_a/mb^2}$
$s$	span of the flat plate model
$S_a$	static moment of the model about the elastic axis
$t_c$	thickness of the flat plate model
$U$	mean wind tunnel velocity
$U_c$	critical velocity
$U/U_c$	relative velocity

$U/b\omega_\alpha$	reduced velocity
$x_\alpha$	distance in semi-chord from the elastic centre to the centre of gravity, $x_{CG}/b$
$x_{CG}$	distance from the elastic axis (EA) to the centre of gravity (CG), positive toward the trailing edge
$\alpha$	pitch angle about the elastic axis (positive nose-up)
$\alpha_0$	initial condition in pitch
$\alpha_{LCO}$	amplitude in pitch at LCO
$\beta_\alpha$	coefficient of cubic spring in pitch
$\xi$	growth (or damping) rate of the response in plunge or pitch
$\eta_\alpha \eta_h$	structural damping ratio in pitch and plunge
$\mu$	solid/fluid mass ratio, $m/(\pi\rho b^2 s)$
$\nu$	kinematic viscosity
$\varphi$	phase angle by which the plunge leads the pitch
$\varphi_{LCO}$	phase angle by which the plunge leads the pitch at LCO
$\omega_\alpha \omega_h$	uncoupled natural frequencies in pitch and plunge
$\omega_1 \omega_2$	natural frequencies of the coupled system
$\omega_h/\omega_\alpha$	ratio of plunge to pitch uncoupled natural frequencies

## 1. Introduction

Among the fluid-structure instabilities that can be experienced by a slender streamlined body in cross flow, classical flutter and stall flutter are probably the most thoroughly investigated. Observed since the early days of flight the classical flutter of airplane wing is a dynamic instability for which self-sustained oscillations of great violence occurs above a critical speed. Often called coupled-mode flutter this instability involves at least two modes of the system and, unlike the stall flutter, its onset does not rely on any flow separation. It can hence be observed on wing with no angle of attack if not properly designed. Theory of flutter

based upon linear unsteady aerodynamic formulations has been successfully developed to predict the critical conditions for the generic case of a two degrees of freedom “pitch-plunge” oscillating wing (Theodorsen, 1935; Sears, 1941). Since those early works the physical explanation of bending-torsion flutter has also been highlighted (see for example Fung, 1955 or Bisplinghoff and Ashley, 1962). It is now well understood that the classical flutter relies on fluid-elastic coupling between the structural modes. Indeed combined plunging and pitching motions can produce, above a critical flow velocity, interactions and phase shifts in a way that energy is transferred from the flow to the structure. Another distinguishing feature of the coupled pitch-plunge flutter is that both frequencies tend to merge near the flutter condition (Dowell et al, 2004).

Even though classical flutter is a well-known phenomenon, few investigations on the post-critical behaviour have been made, except for nonlinear aeroelastic systems encountered in aeronautics (see Dowell et al, 2003). Lee et al (1999) also presented an extensive review of nonlinear aeroelastic studies focusing on one-degree-of-freedom (pure pitch) or two-degree-of-freedom (pitch-plunge) oscillating airfoils. According to those reviews most referenced studies focused on the impact of concentrated structural nonlinearities such as cubic stiffness (Lee and LeBlanc, 1986) or control surface freeplay (Conner et al, 1997) and on the effects of nonlinear aerodynamics due to shock wave motion in transonic flow (Schewe et al, 2003) or stall flutter of airfoil (Ericsson and Reding, 1971).

Unlike classical flutter, stall flutter is a dynamic instability that does not depend on coupling (Naudascher and Rockwell, 1994). This phenomenon is of particular importance for wing operating at high angle of attack (Victory, 1943), for helicopter rotor blades (Ham and Young, 1966) and for wind turbine blades (Hansen et al, 2006). For wing or blade in stall flutter, torsion is the mode of vibration most commonly involved. The mechanism for energy transfer then relies on a dynamic stall process for which the flow separates partially or completely during each cycle of oscillation (Dowell, 2004; Bhat and Govardhan, 2013). Due to the nonlinear nature of the aerodynamic load involved, stall flutter is limited in amplitude (McCroskey, 1982; Li and Dimitriadis, 2007). Many studies have been devoted to the dynamic stall process experienced by a wing oscillating around the static stall angle of attack (McCroskey and Philippe, 1975; Carr et al, 1977) and to the aeroelastic response of a pure pitch or pitch-plunge airfoil in the post critical stall flutter condition (see for example Dunn and Dugundji, 1992; Price & Fragiskatos, 2000; Li and Dimitriadis, 2007; Sarkar and Bijl, 2008; Razak et al, 2011). Among those studies only few have pointed out that classical flutter could also be limited in amplitude. Post-critical LCO have been experimentally observed by Dunn and Dugundji (1992) on a cantilevered wing at low angle of attack but they concluded,

based upon additional numerical calculations, that observed LCO were mainly due to a cubic hardening stiffness effect. Price and Fragiskatos (2000) performed numerical nonlinear aeroelastic studies on a two-degree-of-freedom structurally linear airfoil. They identified LCO beyond the critical velocity and a gradual increase of LCO amplitude with the velocity. They argued that LCO are due to the nonlinear nature of the aerodynamics but they also mentioned that their results should be taken carefully due to the fact that their dynamic stall model had not been validated for high amplitudes. As for stall flutter, it therefore appears that with no structural limitation classical flutter does not grow exponentially but also exhibit limit amplitude oscillation.

In the new and challenging field of energy harvesting through fluid-structure instabilities, the coupled-mode flutter mechanism has been recently scrutinized (Peng and Zhu, 2009; Zhu, 2012; Boragno et al, 2012). A greater focus on post-critical behaviour is however necessary in order to improve the characterization, physical understanding and modeling of the large amplitude self-sustained vibrations resulting from these instabilities. The aim of this paper is to provide experimental results in that context.

The paper is organized as follows: the experimental set-up along with the relevant structural and aerodynamic parameters are presented in section 2. Flutter results are reported in section 3. Frequencies of the aeroelastic modes of the system are first presented for various flow velocities. Results are compared with linear theoretical prediction to confirm the observed critical velocity and coupled-mode flutter. The post-critical behaviour is then characterized, highlighting LCO amplitude and phase evolutions with the flow velocity along with the influence of initial perturbations on the dynamical response of the system.

## **2. Experimental set-up**

The experiments were performed using a rigid flat and rectangular steel plate of span  $s=0.225\text{m}$ , chord length  $c=0.035\text{m}$  and thickness  $t_c=0.0015\text{m}$ , corresponding to a thickness-to-chord ratio of 4.3%. Dimensions are shown in Fig. 1. In order to limit the effect of the Reynolds number, no modification was made on the nose and tail of the model which is characterized by a rectangular cross section.

The flat plate model was flexibly mounted in plunge and pitch in a small Eiffel wind tunnel (Fig. 2), with a closed rectangular test-section of 0.26 m width and 0.24 m height. A particular attention was paid to the design of a set-up that can allow high amplitude linear response in pitch and plunge. The chord dimension of the model was less than 15% of the height of the wind tunnel cross section in order to avoid blockage effects for high amplitude oscillations. End plates were mounted at each extremity of the flat-plate model in order to limit end

effects. The set-up is shown in Figs. 1 and 2. The vertical stiffness of the system was set by two long steel laminated springs and two sets of additional linear springs. In order to limit the structural damping in rotation no bearings were involved in the design and the axis of rotation was linked to the laminated spring by point-tailstock mechanical connections. The rotational stiffness was set by two linear springs (see Figs. 1 and 2) and the elastic axis was fixed at a distance  $x_{cg}$  ahead of the centre of gravity (see Fig. 3).

Tests were performed for a mean velocity in the test-section varying from 5 to 13m/s, with a turbulence level less than 0.4% over this velocity range. In the present study the mean angle of attack of the model is set to zero.

The two degrees of freedom  $h(t)$  and  $\alpha(t)$  were measured using two laser displacement sensors connected to a 24 bits resolution acquisition system. The first one directly measured the vertical plunging motion at the elastic axis, while the second one measured the combined movement in plunge and pitch. Recovery of the physical quantities  $h(t)$  and  $\alpha(t)$  was performed by numerical post-processing with an accuracy less than 2%. The sampling frequency was chosen as 1024Hz and spectral analysis was performed on time block over 8 seconds which gives a frequency resolution lower than 0.125 Hz.

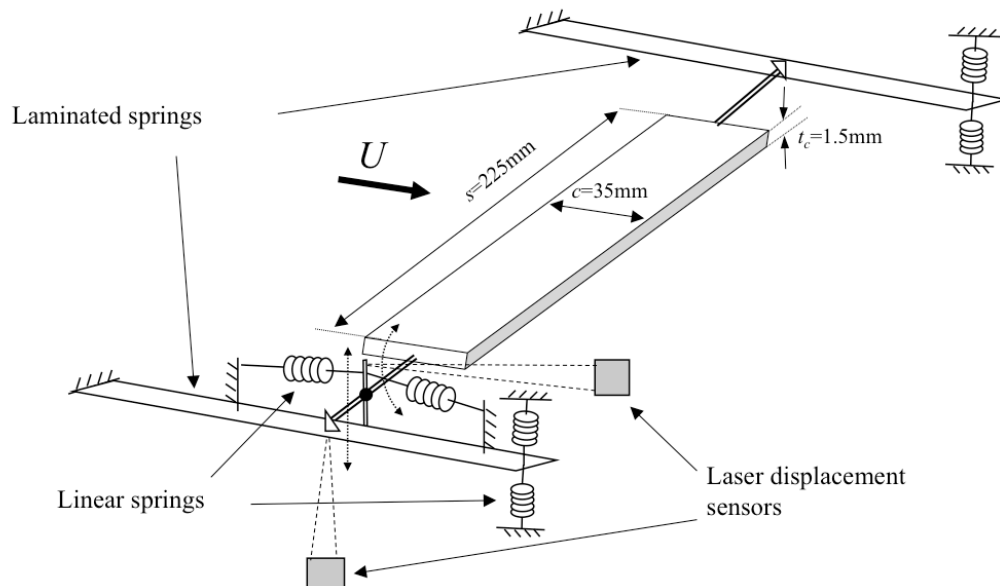


**Fig. 1.** Schematic draw of the experimental set-up.

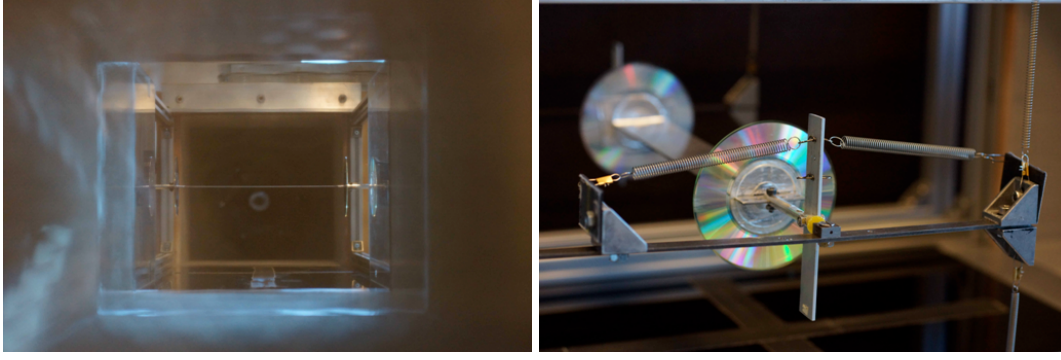


**Fig. 2.** Front view of the flat plate model in wind tunnel (left) and side view of the set-up (right).

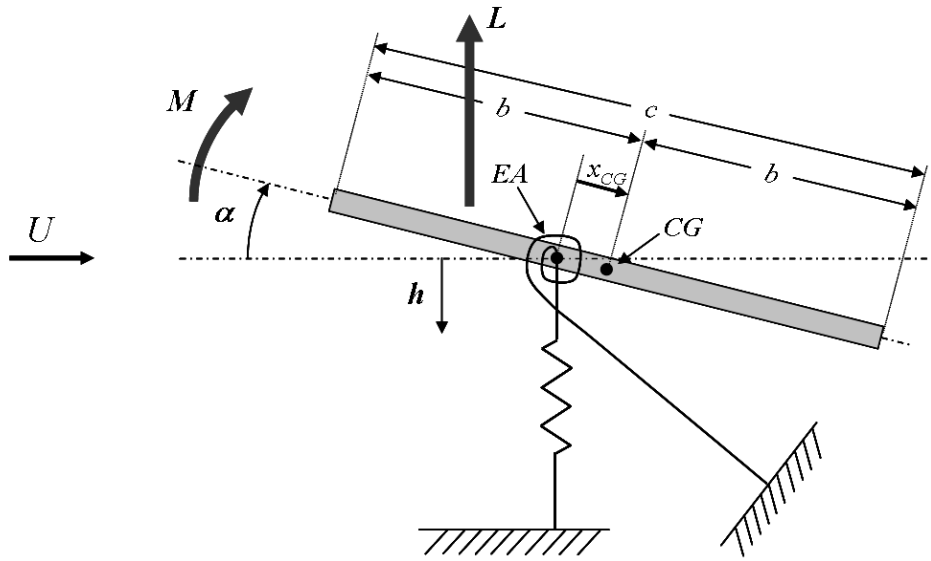


**Fig. 3.** Two dimensional flexibly mounted flat plate section model

### 2.1 Structural parameters

Since the elastic centre was not located at the centre of gravity, the two-degree-of-freedom system (see Fig. 3) was structurally coupled. The linearized equations of motion can then be expressed as following (Fung, 1955):

$$\begin{aligned} m \ddot{h} + D_h \dot{h} + K_h h + S_\alpha \ddot{\alpha} &= -L, \\ I_\alpha \ddot{\alpha} + D_\alpha \dot{\alpha} + K_\alpha \alpha + S_\alpha \ddot{h} &= M, \end{aligned} \quad (1)$$

where the parameters  $m$ ,  $I_\alpha$ ,  $D_h$ ,  $D_\alpha$ ,  $K_h$ ,  $K_\alpha$  are the system's mass, moment of inertia about the elastic axis, structural damping and stiffness in plunge and pitch, respectively.  $S_\alpha = m x_{CG}$  is

the static moment of the flat-plate model about the elastic axis.  $L$  and  $M$  are respectively the aerodynamic lift (positive upward) and pitching moment (positive leading-edge up) about the elastic axis, acting on the flat-plate model.

Structural parameters of the system were identified under zero-wind velocity. A static weight calibration technique was used to measure the stiffness  $K_h$  and  $K_\alpha$ . The force (and torque) versus displacement curves are shown in Fig. 4.

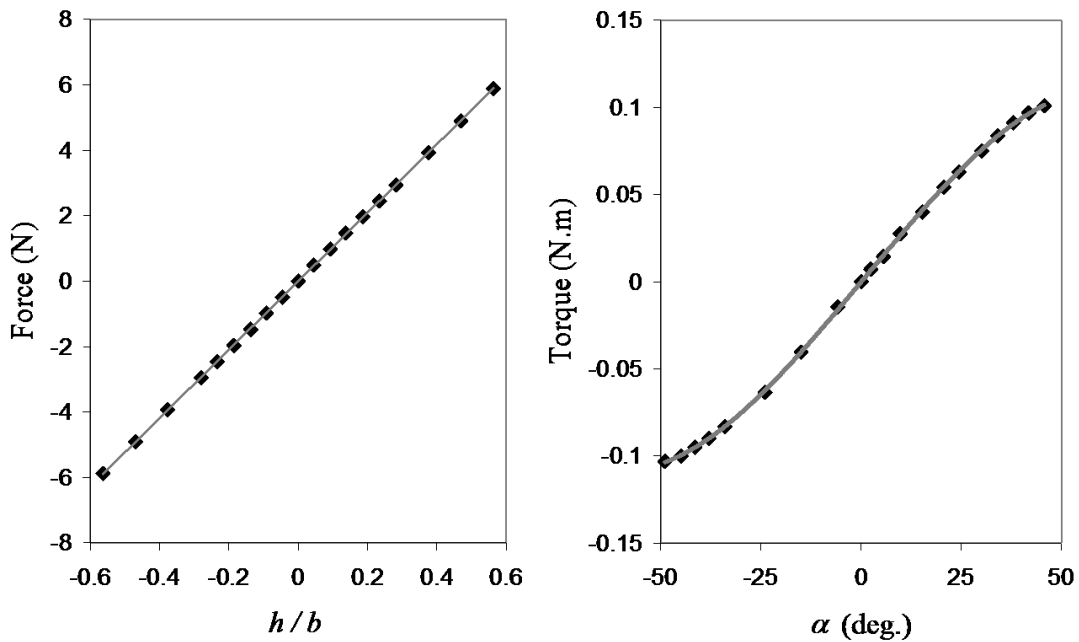


**Fig. 4.** Stiffness static weight calibration in plunge (left) and in pitch (right)

Results show that the bending stiffness behaves linearly in the range  $-0.6 \leq h/b \leq 0.6$ . On the other hand the stiffness in rotation is characterized by a small softening spring behaviour which is well described by the following cubic function for the restoring torque (where  $\beta_\alpha$  is a cubic non linear coefficient):

$$M_K(\alpha) = K_\alpha (\alpha + \beta_\alpha \alpha^3), \quad (2)$$

$$K_\alpha = 0.149, \quad \beta_\alpha = -0.248.$$

Therefore, the stiffness in rotation has a quasi-linear behaviour in the range  $-25 \text{ deg} \leq \alpha \leq 25 \text{ deg}$ , with a departure from the linear behaviour smaller than 6% for  $\alpha \approx 25 \text{ deg}$ . For higher angles of rotation the stiffness smoothly reduces and for  $\alpha \pm 50$  degrees the restoring torque is 19% lower than its linear approximation.

Free decay tests under zero wind conditions were performed for each degree of freedom taken independently (the other one being locked). Natural frequencies  $\omega_h$  and  $\omega_\alpha$  are then obtained by spectral analysis. Pure structural damping values  $D_h$  and  $D_\alpha$  were determined using a standard decrement technique to assess the damping ratios  $\eta_h = D_h/2\sqrt{K_h m}$  and  $\eta_\alpha = D_\alpha/2\sqrt{K_\alpha I_\alpha}$ . Non dimensional values reported in Table 2 show that the damping ratio is very small in plunge  $\eta_h \approx 0.2\%$  and significantly higher in pitch  $\eta_\alpha \approx 1.5\%$ . Free decay tests were performed for different amplitudes of initial conditions up to  $h_0/b \approx 0.6$  and  $\alpha_0 \approx 40$  deg. Results showed that the structural damping behaves linearly in plunge but significantly increases in pitch for very low angle of attack ( $|\alpha| < 1$  deg), because of the solid friction induced by the point-tailstock connection. As a consequence, a small mechanical initial perturbation was systematically given to the system for the identification of flutter conditions.

Assuming that the structural damping is small, the inertia  $I_\alpha$  and mass  $m$  of the moving parts of the set-up are found, using:

$$\begin{aligned} I_\alpha &= K_\alpha/\omega_\alpha^2, \\ m &= K_h/\omega_h^2. \end{aligned} \tag{3}$$

Free decay tests have also been performed for the two-degrees of freedom system under zero wind conditions. From the measured natural frequencies  $\omega_1$  and  $\omega_2$  of the coupled system one can identify the static unbalance of the section model about the elastic axis using the following expression (see Bisplinghoff and Ashley, 1962):

$$S_\alpha = \sqrt{m I_\alpha \left( 1 - \frac{\omega_h^2 + \omega_\alpha^2}{\omega_1^2 + \omega_2^2} \right)}. \tag{4}$$

Structural parameters of the system are summarized in Tab. 1. The half-chord  $b=c/2$  was chosen as a reference length scale. Associated non-dimensional parameters are reported in Tab. 2 with  $\omega_h/\omega_\alpha$  the ratio of plunge to pitch natural frequencies,  $r_g = \sqrt{I_\alpha/mb^2}$  the non-dimensional radius of gyration of the system about its elastic centre,  $m/(\pi \rho b^2 s)$  the

solid/fluid mass ratio and  $x_\alpha = x_{CG}/b$  the non-dimensional distance from the elastic centre to the centre of gravity (counted positively toward the trailing edge).

**Table 1**

Structural parameters of the system (S.I. units)

$m$	$I_a$	$D_h$	$D_\alpha$	$K_h$	$K_\alpha$	$\omega_h$	$\omega_\alpha$	$S_\alpha$	$x_{CG}$
0.304	$4.66 \times 10^{-5}$	$5.38 \times 10^{-2}$	$7.91 \times 10^{-5}$	595.6	0.149	44.26	56.55	$8.48 \times 10^{-4}$	$2.8 \times 10^{-3}$

**Table 2**

Non dimensional parameters of the system

$\omega_h/\omega_\alpha$	$r_g$	$\mu$	$\eta_h$	$\eta_\alpha$	$x_\alpha$
0.783	0.707	1170.3	0.002	0.015	0.159

## 2.2 Flat plate steady aerodynamic results

In situ measurements of the lift and moment coefficients of the flat plate model were performed using a static weight calibration technique under a wind velocity  $U \approx 10$  m/s (i.e. a Reynolds number close to  $2.3 \times 10^4$ ) at various angles of attack. Results are compared in Fig. 5 with the experiments of Fage and Johansen (1927) on a sharp-edged flat plate of thickness-to-chord ratio of 3% at  $Re \approx 10^5$ , along with those of Pelletier and Mueller (2000) on a flat plate model of thickness-to-chord ratio of 1.93% at  $Re \approx 8 \times 10^5$ . The pitching moment reported in Fig. 5 is defined about the mid-chord.

In the low-angle linear region ( $\alpha < 5$  deg), results are consistent with the thin airfoil theory. The slopes of the lift curve and moment curve are obtained as  $dC_L/d\alpha \approx 6.2$  and  $dC_{M,mc}/d\alpha \approx 1.4$ , respectively, which corresponds to an aerodynamic centre location close to the first quarter chord. A smooth stall (gradual reduction of the lift-curve slope) occurs for  $\alpha > 7$  deg. According to Fage and Johansen (1927) the flat plate is characterized by a leading-edge laminar separation bubble at very low angle of attack. Its length (from the leading edge to the reattachment point) increases gradually with the angle of attack until complete separation from the upper surface for a static stall angle close to 7.5 deg. In the present study the stall angle of attack is slightly lower which gives lower lift coefficients for  $7 \text{ deg} < \alpha < 13$  deg. However the moment coefficient agrees well with the results of Fage & Johansen in the same range of angle of attack, with an abrupt decrease for  $\alpha \approx 7-8$  deg which is due to the combination of a stalled lift coefficient and a centre of pressure location moving toward the

mid-chord. At high angle of attack  $13 \text{ deg} < \alpha < 60 \text{ deg}$ , the measured lift coefficient also agrees well with the results of Fage & Johansen but also reveals another “stall” behaviour for  $16 \text{ deg} < \alpha < 19 \text{ deg}$ .

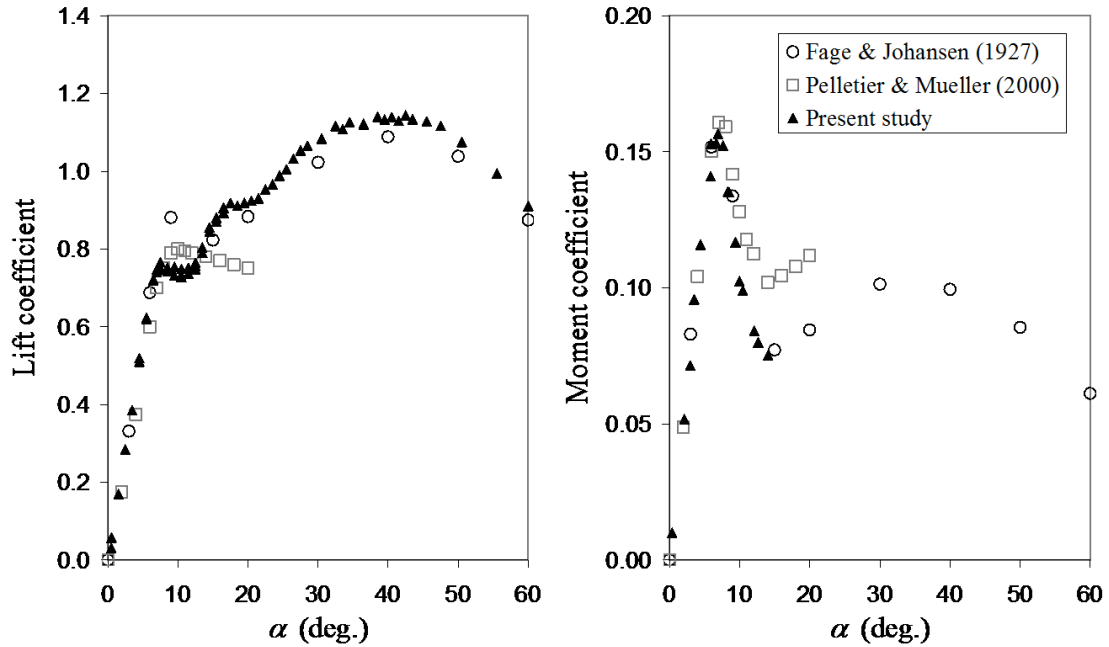


**Fig. 5.** Flat plate lift coefficient ( $C_L$ ) and moment coefficient about the mid-chord ( $C_{M,mc}$ ) versus angle of attack. (Open circles): Fage and Johansen (1927),  $Re \approx 10^5$ ; (open squares): Pelletier and Mueller (2000),  $Re \approx 8 \times 10^5$ ; (filled triangles): present study,  $Re \approx 2.3 \times 10^4$ .

### 3. Low speed flutter results

Experiments were performed with the flat plate model at zero mean angle of attack for a wind tunnel velocity ranging from 5 up to 13m/s (i.e.  $1.17 \times 10^4 < Re < 3.03 \times 10^4$ ). When the flow velocity is increased the system remains stable to any small initial perturbations up to a critical velocity  $U_c \approx 10.5 \text{ m/s}$  ( $Re \approx 2.45 \times 10^4$ ). Beyond this critical velocity the system undergoes a coupled-mode flutter instability characterized by limit cycle oscillations that were studied up to  $U/U_c \approx 1.2$ . For higher velocities the dynamics of the system are corrupted by a static divergence in the pitching degree of freedom due to the structural limitation of the experimental set-up.

#### 3.1 Frequencies evolution with the flow-velocity

Free decay tests have been performed for various velocities in stable and post-stable conditions. Spectral analysis of the dynamical responses was used to identify the frequencies

of both aeroelastic modes of the system as a function of the wind velocity. Dimensionless results are reported in Fig. 6.

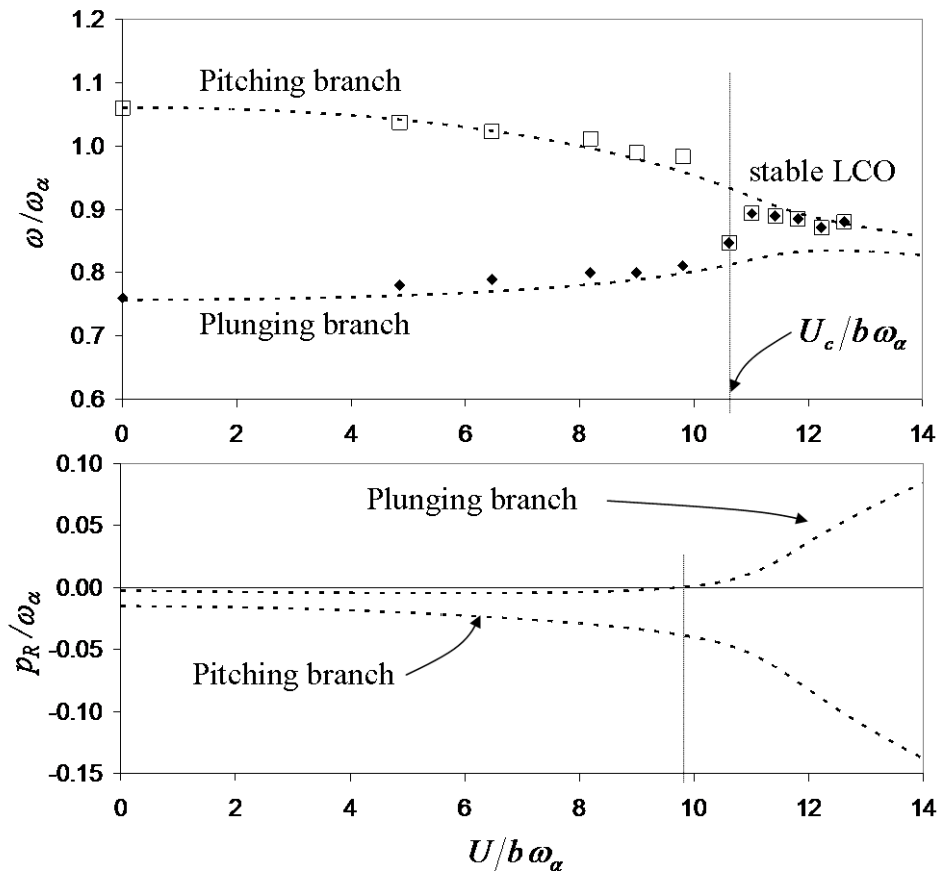


**Fig. 6.** Dimensionless frequencies  $\omega / \omega_\alpha$  and growth rate  $p_R / \omega_\alpha$  of the aeroelastic modes of the system versus reduced velocity. (Open squares and filled diamond): experimental results; dashed line: linear theoretical prediction (see section 3.2)

For reduced velocities  $U/b\omega_\alpha > 4$  both frequencies smoothly approach each other (the plunging frequency increasing while the pitching one decreases). For  $U/b\omega_\alpha \approx 10.6$ , responses in plunge and pitch are dominated by a single frequency  $\omega/\omega_\alpha \approx 0.85$ . This point corresponds to the critical condition ( $U=U_c$ ) for which the system is unstable to any small initial perturbations and starts to flutter. For higher velocities the system exhibits stable quasi-harmonic LCO for which the frequency is significantly higher but slightly reduces with the wind velocity to reach  $\omega/\omega_\alpha \approx 0.88$  for  $U/U_c \approx 1.2$ .

### 3.2 Linear flutter prediction; eigenvalues evolution with the flow-velocity

Dynamic eigenvalues of the two-degree-of-freedom aeroelastic system was calculated

using Eq. (1) and the linear Theodorsen's formulation for the motion-induced lift and moment (Theodorsen, 1935):

$$\begin{aligned}\frac{L}{\rho b U^2 s} &= \pi \left\{ \frac{b\dot{\alpha}}{U} + \frac{b}{U^2} \ddot{h} - \frac{ab^2}{U^2} \ddot{\alpha} \right\} + \frac{dC_L}{d\alpha} C(k) \left[ \alpha + \frac{\dot{h}}{U} + \left( \frac{1}{2} - a \right) \frac{b\dot{\alpha}}{U} \right], \\ \frac{M}{2\rho b^2 U^2 s} &= \frac{\pi}{2} \left\{ \frac{ab}{U^2} \ddot{h} - \frac{b^2}{U^2} \left( \frac{1}{8} + a^2 \right) \ddot{\alpha} + \left( a - \frac{1}{2} \right) \frac{b\dot{\alpha}}{U} \right\} + \frac{dC_M}{d\alpha} C(k) \left[ \alpha + \frac{\dot{h}}{U} + \left( \frac{1}{2} - a \right) \frac{b\dot{\alpha}}{U} \right].\end{aligned}\quad (5)$$

Introducing the parameter  $a = x_{CG}/b$  which is the distance in semi-chord from the mid-chord to the elastic axis, the lift and moment coefficient derivatives around zero angle of attack ( $dC_L/d\alpha$  and  $dC_M/d\alpha$ ), and the so-called Theodorsen's function  $C(k)$  which is a complex function of the reduced frequency  $k = \omega b/U$  for which an exact expression can be found in Fung (1955).

For each flow velocity one can then calculate two oscillatory root pairs, each of the form  $p = p_R \pm i\omega$  associated to the determinant of the aeroelastic system expressed in the Laplace transform variable (see Bisplinghoff and Ashley, 1962, for more details). Calculations were performed using the lift coefficient slope identified experimentally,  $dC_L/d\alpha \approx 6.2$  and a moment curve slope corrected for an elastic axis at a distance  $x_{CG}$  ahead of the mid-chord :  $dC_M/d\alpha \approx 0.91$ . Dimensionless frequencies  $\omega/\omega_\alpha$  and associated growth rate  $p_R/\omega_\alpha$  are reported in Fig. 6 in the velocity range of the experimental results.

Theoretical predictions are observed to be in very good agreement with the experiments. They also confirm that the onset of instability is due to an aeroelastic mode associated with the plunging branch. Moreover the linear stability analysis predict a critical flutter velocity (for which the plunging branch growth rate becomes positive)  $U_c/b\omega_\alpha \approx 9.8$  which is slightly lower than the one observed experimentally  $U_c/b\omega_\alpha \approx 10.6$ . One can also notice that beyond the critical velocity the coupled-mode flutter frequencies which have been measured are very close to the theoretical pitching branch.

### 3.3 Analysis of the dynamical response

Below the critical velocity, i.e. for  $U/b\omega_\alpha < 10.6$ , plunging and pitching responses to any small initial perturbation are both damped to reach a small turbulence-induced vibration regime ( $h/b < 0.005$  &  $\alpha < 0.1$  deg.).

At the critical velocity ( $U_c/b\omega_\alpha \approx 10.6$ ) the system is unstable and any small initial perturbation is amplified. Plunging and pitching responses to an initial deflection in plunge  $h_0/b \approx 0.18$  are reported on Fig. 7. The associated phase diagram is presented in Fig. 11.

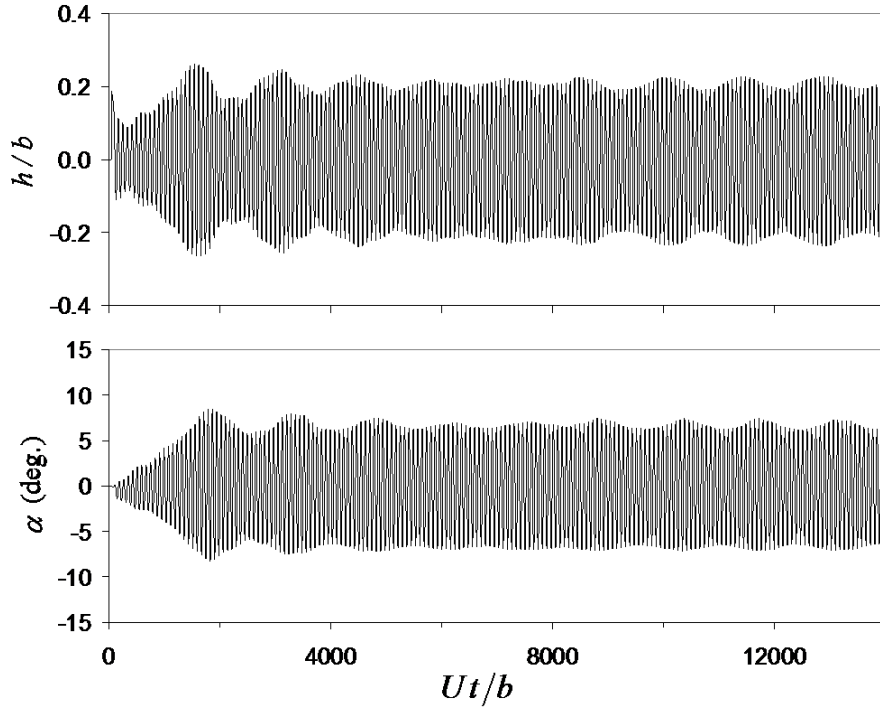


**Fig. 7.** Evolution of the plunge and pitch with non-dimensional time  $Ut/b$  at the critical velocity  $U_c/b\omega_\alpha \approx 10.6$

After a small transient regime the vibrations in pitch and plunge both increase until the non-dimensional time reach  $Ut/b \approx 1.7 \times 10^3$  where the oscillation amplitudes saturate. One can then observe a limit-cycle oscillation regime with an amplitude varying slowly in time. For  $Ut/b > 4 \times 10^3$  the LCO amplitudes in plunge and pitch are  $h_{LCO}/b \approx 0.22 \pm 0.04$  and  $\alpha_{LCO} \approx 6.5 \pm 0.5$  deg.

Fig. 8 shows the evolution with time of the growth (or damping) rate  $\zeta$  of both the plunging and pitching response along with the phase angle  $\varphi$  by which the plunge leads the pitch. Each point  $\zeta$  was identified from the natural log difference of the amplitude of any two successive peaks (maximum or minimum) in plunge or pitch:

$$\zeta_{\alpha,i} = \frac{\delta_{\alpha,i}}{\sqrt{(2\pi)^2 + (\delta_{\alpha,i})^2}}, \quad \zeta_{h,i} = \frac{\delta_{h,i}}{\sqrt{(2\pi)^2 + (\delta_{h,i})^2}}, \quad (6)$$

$$\delta_{\alpha,i} = \ln(\alpha_{\max,i+1}) - \ln(\alpha_{\max,i}), \quad \delta_{h,i} = \ln(h_{\max,i+1}) - \ln(h_{\max,i}).$$

With those definitions any growth (or damping) rate value can be directly compared to structural damping ratios  $\eta_h$  or  $\eta_\alpha$ . The evolution of the phase shift  $\varphi$  has been identified considering the time delay between any two successive peaks (maximum or minimum) in pitch and plunge:

$$\varphi_i = (t_{\alpha_{\max},i} - t_{h_{\max},i}) \times \omega \text{ or } \phi_i = (t_{\alpha_{\min},i} - t_{h_{\min},i}) \times \omega. \quad (7)$$

With this definition  $\varphi$  is the phase angle by which the plunging motion leads the pitching motion, assuming that both pitch and plunge can be locally approximated by quasi harmonic expressions:  $h(t) \approx \tilde{h} \cos(\omega t + \varphi)$  and  $\alpha(t) \approx \tilde{\alpha} \cos(\omega t)$ .

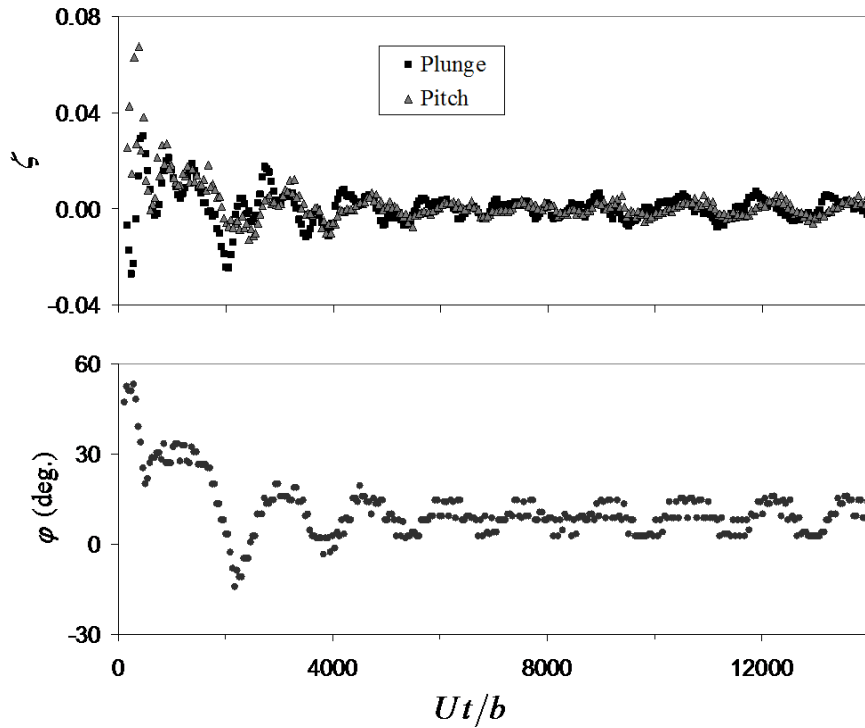


**Fig. 8.** Time history of the growth (or damping) rate  $\zeta$  in pitch and plunge and phase angle  $\varphi$  between the plunge and the pitch;  $U_c/b\omega_\alpha \approx 10.6$

Starting from rest with an initial deflection  $h_0/b \approx 0.18$  the plunging oscillation amplitude first decreases ( $\zeta \approx -2\%$ ) while the pitching amplitude strongly increases ( $\zeta > 5\%$ ). After 3 cycles for which  $\varphi \approx 50$  deg, both the pitch and plunge exhibit positive growth rate  $0 < \zeta < 3\%$  with an associated phase shift  $\varphi \approx 30$  deg. For  $1.7 \times 10^3 < Ut/b < 4 \times 10^3$  significant oscillations of  $\zeta$  ( $\pm 2\%$ ) and  $\varphi$  (between  $-20$  deg and  $20$  deg) are responsible for the amplitude modulations in pitch and plunge. For  $Ut/b > 4 \times 10^3$  the limit-cycle oscillations regime is characterized by a mean phase angle  $\varphi_{LCO} \approx 10$  deg. Fig. 8 also show that the slow time varying amplitude observed in Fig. 7 is due to the phase angle fluctuation from  $\varphi \approx 20$  deg (maximum growth) to  $\varphi \approx 0$  deg (in phase regime for which the system is damped).

For higher velocities, the dynamical response changes dramatically. This can be seen in Fig. 9 for a relative velocity  $U/U_c \approx 1.08$ . After an initial transient growth of mechanical energy a first regime of low amplitude oscillations in pitch ( $\alpha < 11$  deg) is observed for  $2.2 \times 10^3 < Ut/b < 2.8 \times 10^3$ . At the same time the response in plunge strongly decreases before growing again along with the pitching oscillations. The system then branches-off to a higher and stable limit cycle oscillations regime characterized by large harmonic oscillations:  $h_{LCO}/b \approx 0.4 \pm 0.05$  and  $\alpha_{LCO} \approx 34 \pm 1$  deg. The associated phase diagram (Fig. 11) also shows a switch of the phase angle between the pitch and the plunge from the initial transient growth regime to the high limit cycle oscillations regime.

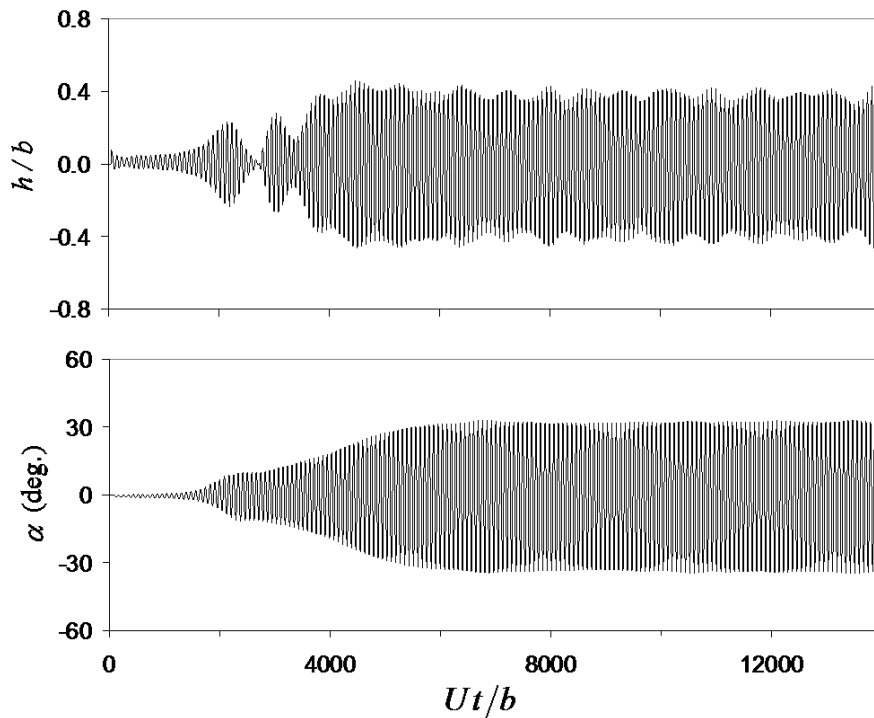


**Fig. 9.** Time response in plunge and pitch in the post critical regime  $U/U_c \approx 1.08$

This is confirmed in Fig. 10 showing the time history of the plunging and pitching growth rates along with the evolution of the phase shift  $\varphi$ . In the initial transient growth regime the phase angle  $\varphi$  increases from 20 deg ( $Ut/b \approx 0.5 \times 10^3$ ) to 60 deg ( $Ut/b \approx 1.8 \times 10^3$ ) where the growth rate is maximum ( $\zeta \approx 3\%$ ). For  $2.2 \times 10^3 < Ut/b < 2.8 \times 10^3$  the phase shift  $\varphi$  gradually decreases to reach  $\varphi \approx -80$  deg for  $Ut/b \approx 2.7 \times 10^3$  and then suddenly drop down to  $\varphi \approx 90$  deg. This quadrature phase shift between the plunge and the pitch is associated to a new growth of oscillations leading to high LCO characterized by a mean phase angle  $\varphi_{LCO} \approx 145$  deg.

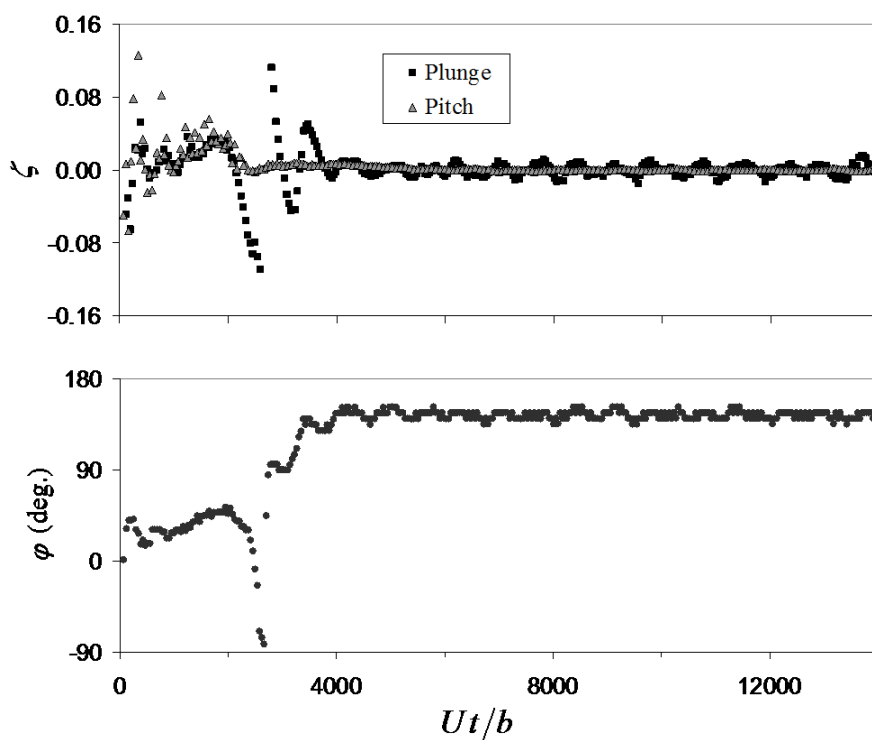


**Fig. 10.** Time history of the growth (or damping) rate  $\zeta$  in pitch and plunge and phase angle  $\varphi$  between the plunge and the pitch;  $U/U_c \approx 1.08$

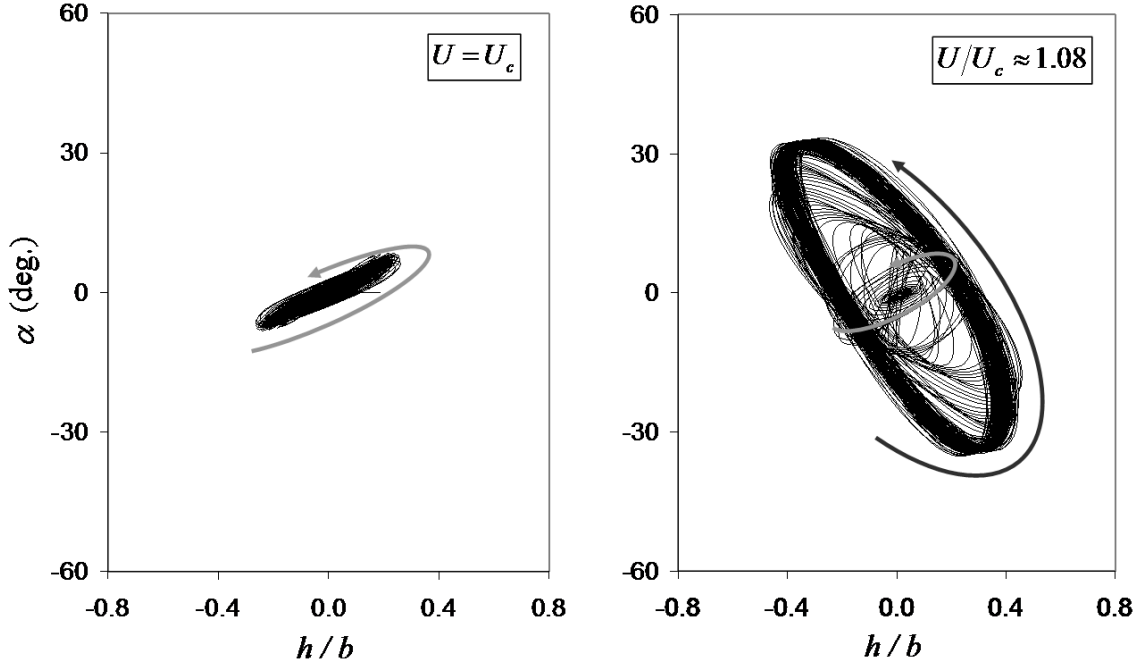


**Fig. 11.** Phase diagram of the dynamical response for  $U=U_c$  and  $U/U_c \approx 1.08$

### 3.4 Evolution of the limit cycle amplitude and phase angle with the wind velocity

For each velocity beyond the critical flutter condition the amplitudes of oscillations associated to stable LCO regime were measured along with the mean phase angle between the pitch and the plunge response. Results are reported in Figs. 12 and 13. On those figures the first set of results was obtained for the system undergoing flutter from rest. Additional tests were also performed decreasing or increasing the flow velocity from a stable high amplitude LCO point. For decreasing flow velocity, results clearly show a hysteretic behaviour of the system which remains in a high amplitude LCO down to a relative velocity  $U/U_c \approx 0.85$ . For lower velocity the system is damped. Increasing the velocity from a stable LCO position at  $U/U_c \approx 0.86$ , the same LCOs have been observed with amplitudes that linearly increase with the relative velocity, reaching  $h_{LCO}/b \approx 0.5$  and  $\alpha_{LCO} \approx 44$  deg at  $U/U_c \approx 1.2$ .

As shown in Fig. 13 the mean phase angle also changes with the velocity ratio. Starting from  $U/U_c \approx 1.2$  for which  $\varphi_{LCO} \approx 60$  deg, and decreasing the flow velocity, the phase gradually increases to  $\varphi_{LCO} \approx 170$  deg for the lower relative velocity  $U/U_c \approx 0.85$ .

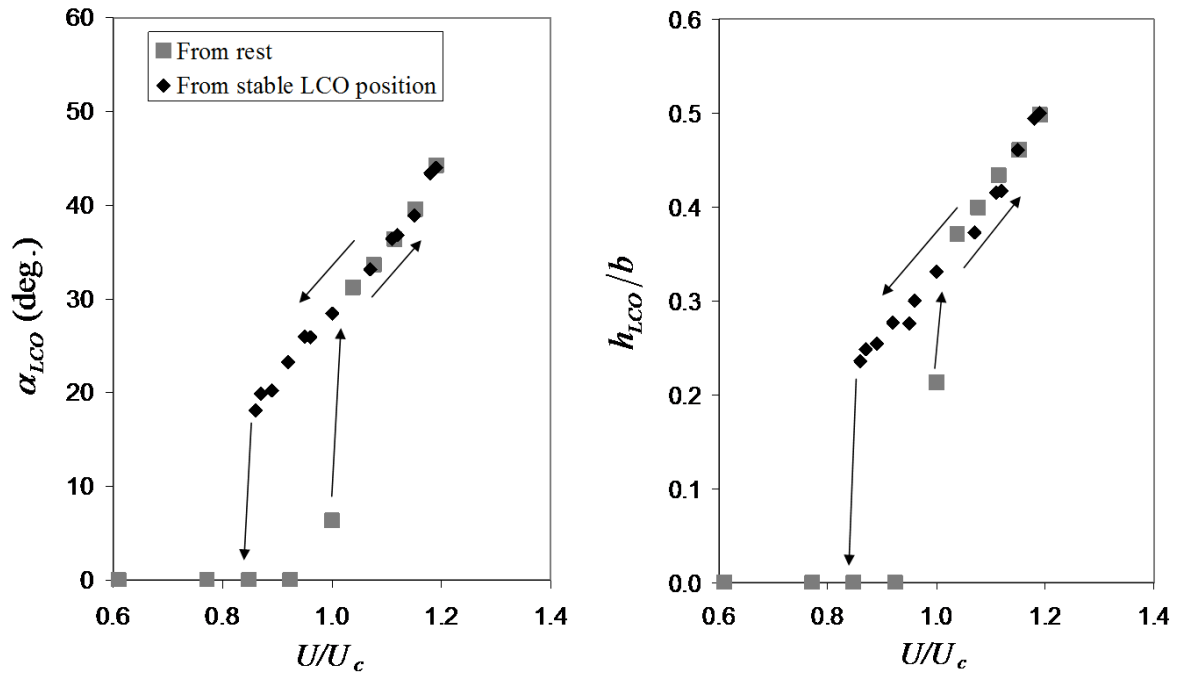


**Fig. 12.** LCO amplitude of the pitching and plunging response versus relative velocity

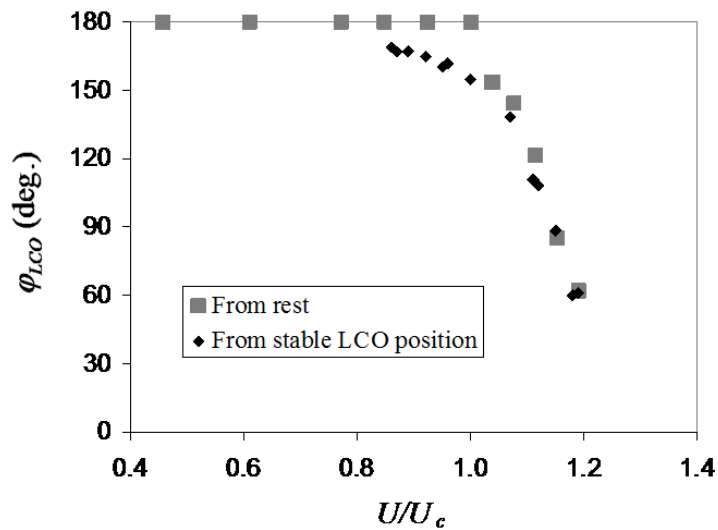


**Fig. 13.** LCO phase evolution with the relative velocity

### 3.5 Effect of initial conditions

LCO observed beyond the linear flutter boundary and the hysteretic behaviour observed for decreasing flow velocity clearly show that the aero-elastic system is subject to nonlinear effects. It is known that initial perturbations can significantly affect the dynamic response of system governed by nonlinear mechanisms. Tests were then performed below and beyond the

critical velocity with different sets of initial conditions.

Below the critical velocity, the system remains stable (i.e. its response is damped) for any low or moderate initial perturbations. Above the critical velocity (i.e. for  $U/U_c > 1$ ) different sets of low, moderate or strong initial conditions have been tested. They showed that even though the transient regime can be significantly affected, the same stable LCO state was reached, with amplitudes and phase angle values consistent with those reported in Figs. 12 and 13. The stability of the high amplitude LCO branch was also analyzed: for any small perturbation the motion systematically returns to the same LCO after a transient regime. For  $0.85 < U/U_c < 1$ , subcritical transitions have been observed for large perturbations of the system. Indeed the onset of strong vibrations leading to the high amplitude LCO branch can be triggered by initial pitch angle and/or plunge deflection such as :  $\alpha_0 > \alpha_{LCO}$  and/or  $h_0 > h_{LCO}$ . On the other hand, the existence of an unstable subcritical LCO branch for  $0.85 < U/U_c < 1$  was not observed for any of the tested moderate initial perturbations  $\alpha_0 < \alpha_{LCO}$  and/or  $h_0 < h_{LCO}$ . Low amplitude LCO regime was only observed for  $U=U_c$ . For higher velocity, this low amplitude LCO is unstable and systematically branches off to the stable high amplitude LCO.

#### 4. Conclusions

The dynamical response of a two-degree-of-freedom flat plate section model undergoing coupled-mode flutter in a wind tunnel was studied. Tests were performed at low Reynolds number ( $1.17 \times 10^4 < Re < 3.03 \times 10^4$ ) using an experimental set-up that enables high amplitude linear response in pitch and plunge for relative velocity up to  $U/U_c \approx 1.2$ .

Flutter boundaries were studied as well as the post-critical behaviour. Beyond the flutter boundary, stable LCO arise with amplitude increasing with the flow velocity. For  $U/U_c \approx 1.2$ , plunging and pitching amplitudes reach  $h_{LCO}/b \approx 0.5$  and  $\alpha_{LCO} \approx 44$  deg with a mean phase angle by which the plunge leads the pitch,  $\varphi_{LCO} \approx 60$  deg. LCO have also been observed below the critical flutter velocity. Decreasing the velocity from a post-critical LCO position the system remains in a stable LCO branch down to a relative velocity  $U/U_c \approx 0.85$  for which  $h_{LCO}/b \approx 0.24$  and  $\alpha_{LCO} \approx 18$  deg. For  $0.85 < U/U_c < 1$  the system, starting from rest, can also move toward a stable LCO if a significant perturbation is imposed.

Those results clearly show that this two-degree-of-freedom pitch and plunge flat plate aeroelastic system is submitted to nonlinear effects. One may then wonder if structural nonlinearities, aerodynamic nonlinearities or both of them are responsible for this behaviour. Cubic structural nonlinearities in pitch/plunge aeroelastic wing were analytically studied by Woolston et al. (1955) and more recently by Lee and LeBlanc (1986). Using a linear

formulation for the aerodynamics, they both analyzed the effect of hard and soft cubic springs in the torsional degree of freedom on flutter boundaries and post critical behaviour. Results showed that a soft spring can affect the stability boundary of the system, i.e a high initial angle of attack can have a destabilizing effect and trigger the flutter. Meanwhile for a small nonlinear spring constant  $\beta_a = -0.3$ , which is close to that of our system, Lee and LeBlanc (1986) found only a small deviation ( $\approx 1\%$ ) from the linear flutter boundary. Furthermore they only observed LCO for hard spring. From these results the soft spring cubic nonlinearity of our system ( $\beta_a \approx -0.25$ ) should have a negligible impact on the flutter boundary results. On the other hand even though it can affect the post-critical response and the observed LCO amplitudes for pitching oscillations beyond  $\pm 25^\circ$ , it cannot be responsible for the saturation mechanism.

As in Price & Fragiskatos (2000) our system seems then to be mainly affected by nonlinear nature aerodynamic effects. Indeed it is interesting that the first saturation highlighted at the critical condition  $U=U_c$  occurs when the angle of rotation reach the static stall angle of attack ( $\alpha \approx 7-8$  deg.). For higher velocity, the system branches off to higher and more stable LCO. Nonlinear dynamic stall conditions can then be responsible for the new saturation in amplitude but further investigations are needed to characterize the mechanisms involved.

## **Acknowledgements**

The authors gratefully acknowledge Electricité de France (EDF) for their support through the ‘Chaire Energies Durables’ at the Ecole polytechnique. S. M. was also supported by a Marie Curie International Reintegration Grant within the seventh European Community Framework Program.

## **References**

- Bisplinghoff, R.L., Ashley, H., 1962. Principles of aeroelasticity. John Wiley and Sons, Inc., New-York, N.Y. Also available in Dover Edition.
- Bhat, S.S., Govardhan, R.N., 2013. Stall flutter of NACA 0012 airfoil at low Reynolds numbers. *Journal of Fluids and Structures* 41, 166–174.
- Boragno, C., Festa, R., Mazzino, A., 2012. Elastically bounded flapping wing for energy harvesting. *Applied Physics Letters* 100, 253906 (2012).

Carr, L.W., McAlister, K.W., McCroskey, W.J., 1977. Analysis of the development of dynamic stall based on oscillating airfoil experiments. NASA-TN-D-8382.

Conner, M.D., Tang, D.M., Dowell, E.H., Virgin, L.N., 1997. Nonlinear behavior of a typical airfoil section with control surface freeplay. *Journal of Fluids and Structures* 11(1), 89-109.

Dowell, E., Edwards, J., Strganac, T.W., 2003. Nonlinear Aeroelasticity. *AIAA Journal of Aircraft* 40(5), 857-874.

Dowell, E.H., Clark, R., Cox, D., Curtiss, H.C., Edwards, J.W., Peters, D.A., Scanlan, R., Simiu, E., Sisto, F., Hall, K.C. and others, 2004. *A modern course in aeroelasticity*. Ed. Kluwer, U.S.A.

Dunn, P., Dugundji, J., 1992. Nonlinear stall flutter and divergence analysis of cantilevered graphite/epoxy wings. *AIAA journal* 30(1), 153-162.

Ericsson, L.E., Reding, J.P., 1971. *Unsteady Airfoil Stall and Stall Flutter*. NASA, CR 111906.

Fung, Y.C., 1955. *An introduction to the theory of aeroelasticity*. John Wiley and Sons, Inc., New-York, N.Y. Also available in Dover Edition.

Fage, A., Johansen, F.C., 1927. On the flow of air behind an inclined flat plate of infinite span, in *Proceedings of the Royal Society of London* 116(773) September, pp. 170-197.

Ham, N.D., Young, M.I., 1966. Limit Cycle Torsional Motion of Helicopter Blades due to Stall. *Journal of Sound and Vibration* 4(3), 431-432.

Hansen, M.O.L., Sørensen, J.N., Voutsinas, S., Sørensen, N., Madsen, H.Aa., 2006. State of the art in wind turbine aerodynamics and aeroelasticity. *Progress in Aerospace Sciences* 42(4), 285-330.

Li, J., Dimitriadis, G., 2007. Experimental Study of Stall Induced LCOS of Free-Vibrating

Wings. in Proceedings of the CEAS International Forum on Aeroelasticity and Structural Dynamics, Paper IF-026, Stockholm.

Lee, B.H.K., Price, S.J., Wong, Y.S., 1999. Nonlinear aeroelastic analysis of airfoils: bifurcations and chaos. *Progress in Aerospace Sciences* 35, 205-334.

Lee B.H.K., LeBlanc P., 1986. Flutter analysis of a two-dimensional airfoil with cubic nonlinear restoring force. *Aeronautical Note NAE-AN-36*, NRC No. 25438, National Research Council of Canada.

McCroskey, W.J., Philippe, J.J., 1975. Unsteady viscous flow on oscillating airfoils. *AIAA Journal* 13(1), 71–79.

McCroskey, W. J., 1982. Unsteady airfoils. *Annual Review of Fluid Mechanics* 14, 285–311.

Naudascher, E. Rockwell, D., 1994. *Flow-induced vibrations: An engineering guide*. Ed. Balkema, Netherlands.

Pelletier, A., Mueller, T.J., 2000. Low Reynolds number aerodynamics of low-aspect-ratio thin/flat/cambered-plate wings. *Journal of Aircraft* 37(5), 825-832.

Peng, Z., Zhu, Q., 2009. Energy harvesting through flow-induced oscillations of a foil. *Physics of Fluids* 21, 123602.

Price, S.J., Fragiskatos, G., 2000. Nonlinear aeroelastic response of a two-degree-of-freedom airfoil oscillating in dynamic stall, in: Ziada, S., Staubli, T. (Eds.), *Proceedings of the Seventh International Conference on Flow Induced Vibration*, Rotterdam, The Netherlands, pp. 437–444.

Razak, N.A., Andrianne, T., Dimitriadis, G., 2011. Flutter and stall flutter of a rectangular wing in a wind tunnel. *AIAA Journal* 49(10), 2258-2271.

Sarkar, S., Bijl, H., 2008. Nonlinear aeroelastic behavior of an oscillating airfoil during stall induced vibration. *Journal of Fluids and Structures* 24,757-777.

Sears, W. R., 1941. Some aspects of non-stationary airfoil theory and its practical application. *Journal of the Aeronautical Sciences* 8, 104-108.

Schewe, G., Mai, H., Dietz, G., 2003. Nonlinear effects in transonic flutter with emphasis on manifestations of limit cycle oscillations. *Journal of Fluids and Structures* 18, 3–22.

Theodorsen, T., 1935. General Theory of aerodynamic instability and the mechanism of flutter. NACA Technical Report 496. (also available in ‘A modern view of Theodore Theodorsen’, published by AIAA in 1992.)

Victory, M., 1943. Flutter at High Incidence. Aeronautical Research Committee, Reports and Memoranda No. 2048.

Woolston D.S., Runyan H.L., Byrdsong T.A., 1955. Some effects of system nonlinearities in the problem of aircraft flutter. NACA TN 3539.

Zhu, Q., 2012. Energy harvesting by a purely passive flapping foil from shear flow. *Journal of Fluids and Structures* 34,157-169.